Physics and Chemistry of the Earth 109 (2019) 59–69

Contents lists available at ScienceDirect

Physics and Chemistry of the Earth

journal homepage: www.elsevier.com/locate/pce

Combining a thermal tracer with a transport model to estimate shallow flow velocities

João R.C.B. Abrantes[a,b,*], Rodrigo B. Moruzzi[b,c], João L.M.P. de Lima[a,b], Alexandre Silveira[a,d], Abelardo A.A. Montenegro[e]

[a] MARE - Marine and Environmental Sciences Centre, Department of Life Sciences, Faculty of Sciences and Technology, University of Coimbra, Rua da Matemática, 49, 3004-517, Coimbra, Portugal
[b] Department of Civil Engineering, Faculty of Sciences and Technology, University of Coimbra, Rua Luís Reis Santos, Pólo II - Universidade de Coimbra, 3030-788, Coimbra, Portugal
[c] Geoprocessing and Territorial Planning Department, Geosciences and Mathematics Institute, UNESP – Univ. Estadual Paulista, Avenida 24 A, 1515, Bela Vista, 13506-900, Rio Claro, SP, Brazil
[d] Institute of Science and Technology, Federal University of Alfenas, Rodovia José Aurélio Vilela, 11.999, Campus Avançado de Poços de Caldas, 37701-339, Poços de Caldas, MG, Brazil
[e] Department of Agricultural Engineering, Rural Federal University of Pernambuco, Rua Dom Manoel de Medeiros, Dois Irmãos, 50910-130, Recife, PE, Brazil

ARTICLE INFO

Keywords:
Thermal tracer
Salt tracer
Advection-dispersion transport equation
Shallow flow velocity
Hydraulic flume

ABSTRACT

For a long time, tracer techniques based on dyes, salts and more recently heat have been used to estimate shallow flow velocities. Traditionally, flow velocity estimation using tracers would consist of tracking the movement of the leading edge or the centroid of the tracer with the flow. An alternative methodology uses an analytical solution of an advection–dispersion transport equation as the mathematical foundation for measuring shallow water flow velocity from tracer measurements. The main goal of the present study was to ascertain whether this alternative numerical methodology can be used with temperature data from thermal tracer measurements. Salt and thermal tracer techniques were applied simultaneously by injecting a double tracer of salted-heated water into different shallow flows simulated in a laboratory hydraulic flume. Simulated flows combined different bed surfaces (smooth acrylic sheet, rough sand board and synthetic grass carpet), flow discharges (from 47 to 1239 ml s^{-1}) and bed slopes (0.8, 4.4 and 13.2%), resulting in a wide range of hydraulic conditions. Velocities determined with the abovementioned methodology were compared with those estimated by measuring the tracers' leading edge and centroid and with mean flow velocity calculated using discharge/depth measurements. Results from combining this alternative numerical methodology with thermal tracer data were similar to results from the salt tracer. Also, the proposed alternative numerical methodology predicted the mean flow velocity calculated from discharge/depth measurements better than the measurements of the leading edge and centroid of the tracers.

1. Introduction

Shallow flows can occur in natural and urbanised basins (e.g. hillslopes, drainage systems) and the accurate measurement of their velocity has been of great concern to hydro-environmental researchers since it would help to better understand and model the dynamics of sediment and pollutant transport.

For a long time, tracer techniques have been used to estimate flow velocity. Many people regard them as crude methods compared with far more sophisticated and accurate methods, such as those based on acoustic and ultrasonic technologies (e.g. ADV, ACDP). However, those technologies may have some limitations if used outside their ideal measurement conditions, and therefore they cannot always be used, particularly in the case of very shallow flows with depths of millimetres to a few centimetres. The most common materials used as tracers in flow velocity estimation are dyes (e.g. Abrahams et al., 1986; Dunkerley, 2003; Flury and Flühler, 1993; Holden et al., 2008; Tazioli, 2011) and salts (e.g. Calkins and Dunne, 1970; Comina et al., 2014; Comiti et al., 2007; Day, 1977; Tatard et al., 2008). The movement of the dye with the flow can be seen with the naked eye or using optical

* Corresponding author. Department of Civil Engineering, Faculty of Sciences and Technology, University of Coimbra, Rua Luís Reis Santos, Pólo II - Universidade de Coimbra, 3030-788, Coimbra, Portugal.
E-mail address: jrcbrito@student.uc.pt (J.R.C.B. Abrantes).

https://doi.org/10.1016/j.pce.2018.12.005
Received 9 May 2018; Received in revised form 27 October 2018; Accepted 18 December 2018
Available online 21 December 2018
1474-7065/

recording equipment. The passage of the salt can be detected by an electrical conductivity sensor placed in contact with the flow.

A more recent approach in flow velocity measurement uses thermal tracers (e.g. hot water, ice cubes) that can be detected by an infrared camera (Abrantes et al., 2018; de Lima and Abrantes, 2014; de Lima et al., 2015, 2018; Schuetz et al., 2012; Tauro and Grimaldi, 2017). Results show that thermal tracers can be used to estimate shallow flow velocities, since the results are similar to those given by other traditional and well-established flow velocity measurement techniques, such as dye tracers (Abrantes et al., 2018; de Lima and Abrantes, 2014), salt tracers (Abrantes et al., 2018; Schuetz et al., 2012), current flow meters (Tauro and Grimaldi, 2017) and ADV equipment (de Lima et al., 2015). One advantage of thermal tracers is that the tracer is more visible in the thermal images than the dye tracer is in the optical images. Thermal tracers can be especially useful when vegetation is concealing the measuring area. Another advantage is the possibility of measuring space-averaged flow velocity, which for salt tracers can only be achieved by installing multiple sensors. Some disadvantages of thermal tracers are the equipment costs and tracer handling. Also, thermal tracers have been shown to be less conservative than salt tracers, which can be important for large scale field applications (e.g. hillslope scale).

Traditionally, flow velocity estimation using tracers would involve measuring the time from the injection of the tracer to its arrival at a sampling point and then dividing this figure by the travel distance. With dyes, the velocity of the leading edge is usually measured. With salts, either the leading edge or centroid of the tracer's concentration at the sampling point is usually measured. The leading edge is regarded as the surface flow velocity and the centroid is regarded as the mean theoretical flow velocity. However, the non-conservative aspects of the tracers, such as advection and diffusion processes, infiltration and constant exchanges between the soil surface and water flow, mean that none of the measured velocities can be considered the actual mean flow velocity. Therefore, correction factors have to be applied to obtain the mean flow velocity (Horton et al., 1934). Such correction factors vary with the flow characteristics (e.g. velocity, depth, regime) and bed surface characteristics (e.g. slope, roughness), as studied in Abrantes et al. (2018), Dunkerley (2001), Emmett (1970), Li and Abrahams (1997), Li et al. (1996), Planchon et al. (2005) and Zhang et al. (2010).

An alternative methodology for determining shallow flow velocities based on the advection-dispersion solute transport model was proposed in Lei et al. (2005). This numerical technique consists of fitting the analytical solution of the differential equation for solute transport in shallow flows to solute transport data obtained by means of a salt tracer, i.e. the solute is a salt and its transport in flow is detected by means of electrical conductivity sensors. This fitting is done by minimising the sum of squared errors between modelled and experimentally observed data. This method has been used in a number of studies involving the determination of shallow flow velocity (Ban et al., 2016; Chen et al., 2017; Huang et al., 2018; Lei et al., 2010, 2013; Rahma et al., 2013; Shi et al., 2012, 2016; Zhuang et al., 2018); it estimates flow velocity more accurately and shows high stability relative to more traditional tracer techniques (e.g. measuring the leading edge or centroid of the tracer). This methodology takes into account the physical processes of advective transport caused by the shifting of the solute field (i.e. concentrated particles) due to the flow movement and diffusive transport by which solute from particles of higher concentration is transferred to particles of lower concentration that are in physical contact (Flick's law).

The main goal of the present study was to ascertain whether the numerical methodology proposed in Lei et al. (2005) could be adapted to temperature data obtained from thermal tracer experiments, first shown in Abrantes et al. (2018). In fact, as with solute transport, heat transport in flowing water is governed by advective transport caused by the translation of the energy field (i.e. heated particles) as result of the flow movement and diffusive transport due to the transfer of energy from higher temperature particles to lower temperature particles that are in physical contact (Fourier's law). Therefore, heat transport in flowing water can be described using a differential transport equation that takes both diffusive and advective transport into account, such as the one used for solute transport.

The analogy of comparison between solute and heat transport has been made in previous investigations. Schuetz et al. (2012) used thermal imaging and injections of heated-salted water as an artificial tracer method to experimentally characterise the spatial distribution of flow paths and to assess solute transport properties in shallow water in a constructed wetland. They found that, at relatively small temporal and spatial scales, heated water can be regarded as a conservative tracer with similar behaviour to salt tracer, and it allows the quantitative determination of transport parameters such as flow velocity and hydrodynamic dispersion. Comparing salt and thermal tracer techniques, Abrantes et al. (2018) observed that, for a small measuring section, the transport of heat and solute was similar and differences between the two tracers were insignificant. The studies by Schuetz et al. (2012) and Abrantes et al. (2018) show that differences between the salt and thermal tracers' conservative properties are of the same magnitude as method errors (e.g. different response times of the equipment, different measurement temporal frequency of the equipment, differences between initial tracer temperature and concentration).

Numerical studies of solute and heat transport in saturated porous media (i.e. groundwater flow) were performed by e.g., de Marsily (1986), Rau et al. (2012) and Vandenbohede et al. (2009). Here, the same advection-dispersion transport model was used for both solute and heat transport. Differences between solute and heat transport are simulated by the hydrodynamic and thermal dispersion coefficients that represent both advective and diffusive transport mechanisms. In these situations (i.e. groundwater flow in porous media) the similarity between heat and solute transport is an approximation that may lack some precision because mass diffusion is orders of magnitude greater in water than in minerals, whereas thermal diffusion is comparable in the two media. However, in the present study, a single medium is considered (i.e. surface shallow flowing water) and therefore differences between media are not important. Furthermore, in such shallow flowing water with high flow rates, solute and heat transport processes are advection dominated (i.e. the effect of the mechanical advection greatly exceeds that of the molecular diffusion), and hydrodynamic and thermal dispersivity coefficients due to advection are considered to be approximately equal.

For the purpose of this study, the analytical solution of the differential advection-dispersion transport equation in shallow flows was fitted both to electrical conductivity data obtained with an electrical conductivity sensor (salt tracer technique) and to temperature data obtained with an infrared video camera (thermal tracer technique). The tracer techniques were applied simultaneously by injecting a double tracer of salted-heated water into different shallow flows simulated in a laboratory hydraulic flume. Simulated flows combined different bed surfaces (smooth acrylic sheet, rough sand board and synthetic grass carpet), flow discharges (from 47 to 1239 ml s^{-1}) and bed slopes (0.8, 4.4 and 13.2%), resulting in a wide range of hydraulic conditions. Velocities determined with the above mentioned methodology were compared with those estimated from measuring the tracers' leading edge and centroid and with mean flow velocity calculated using discharge/depth measurements.

With this adapted methodology the authors seek to combine the advantages of the thermal tracers shown in Abrantes et al. (2018), de Lima and Abrantes (2014), de Lima et al. (2015), Schuetz et al. (2012) and Tauro and Grimaldi (2017) with the advantages of the numerical methodology proposed in Lei et al. (2005).

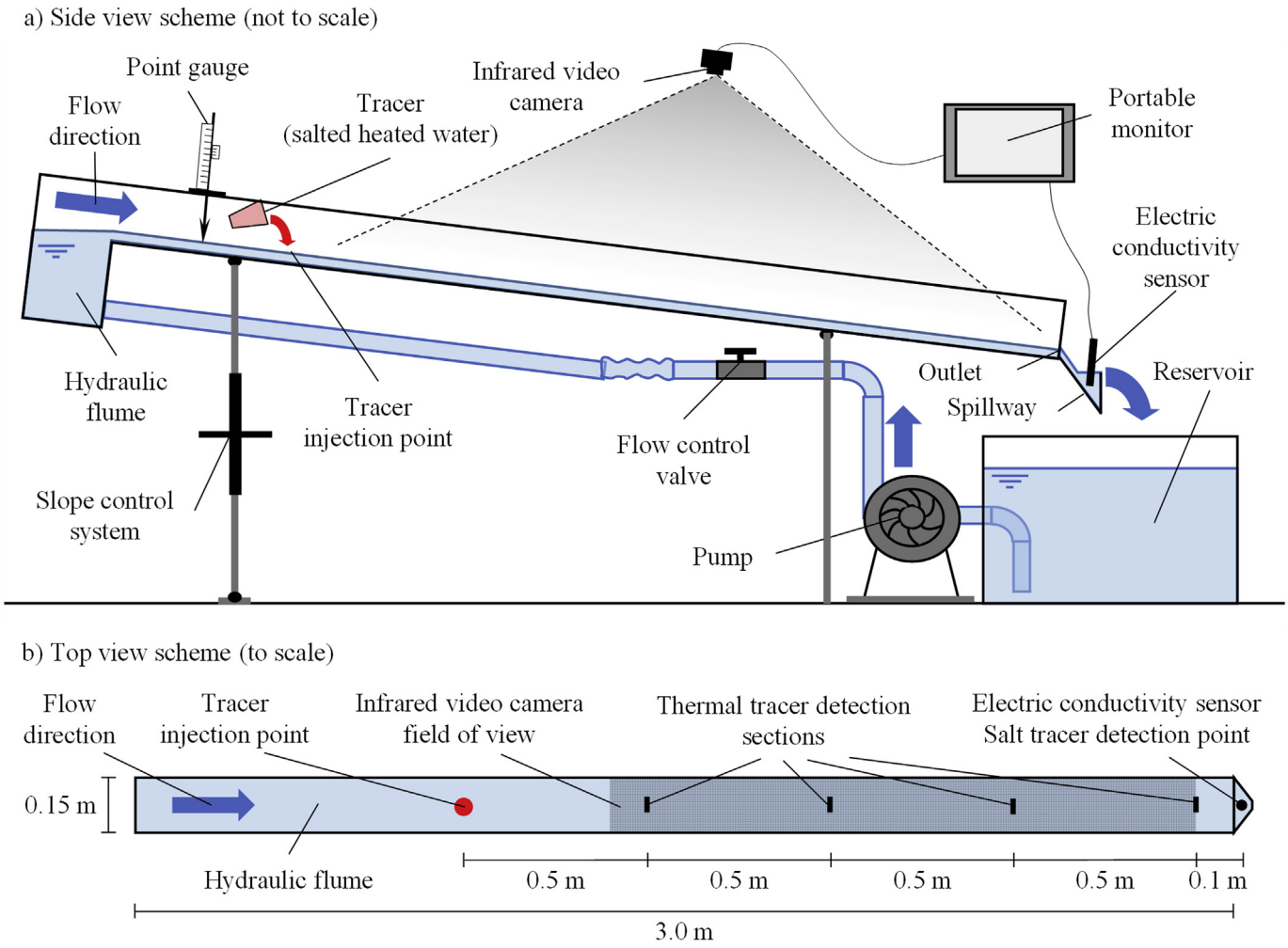

Fig. 1. Schematic representation of the laboratory setup used in the experiments: a) Side view (not to scale); b) View from above (to scale).

2. Methodology

2.1. Solute and heat transport model

The transport of a solute or heat in flowing water is a complicated process that occurs under the influence of both advection and diffusion. It can be defined in general terms by a one-dimensional (1D) differential advection-dispersion transport equation, assuming steady flow (i.e. constant flow velocity and discharge), as follows:

$$\frac{\partial G}{\partial t} = \frac{\partial}{\partial x}\left(D\frac{\partial G}{\partial x}\right) - U\frac{\partial G}{\partial x} \quad (1)$$

where G represents either the solute concentration (C in kg m^{-3}, proportional to the electrical conductivity, EC in µS cm^{-1}) governed by the Fick's law of solute transport or the tracer temperature (T in ºC) governed by Fourier's law of heat transport, D represents either the hydrodynamic dispersion coefficient (D_H in m^2 s^{-1}) or the thermal dispersion coefficient (D_T in m^2 s^{-1}), U is the flow velocity (in m s^{-1}) and represents the movement of the heat or solute with the flow, x is the distance to the solute injection point in the flow direction (in m) and t is time from the instant of solute injection (in s).

2.2. Analytical solution, initial and boundary conditions

An analytical solution to Eq. (1) that uses the Laplace's transformation, is given in Lei et al. (2005). In general terms:

$$G(x, t) = G_0 \frac{x}{2t\sqrt{\pi D \times t}} \exp\left(\frac{U \times x}{2D}\right) \exp\left(-\frac{U^2 t}{4D}\right) \exp\left(-\frac{x^2}{4D \times t}\right) \quad (2)$$

with the following initial (Eq. (2a)) and boundary (Eq. (2b)) conditions:

$$G(x, 0) = 0, \quad \text{for} \quad x \geq 0 \quad (2a)$$

$$G(0, t) = G_0 \times \delta(t) \quad \text{and} \quad G(\infty, t) = 0, \quad \text{for} \quad t > 0 \quad (2b)$$

where G_0 represents either the amount of injected solute concentration (C_0 in kg s m^{-3}, proportional to the electrical conductivity, EC_0 in µS s cm^{-1}) or the amount of injected tracer temperature (T_0 in ºC s) and δ(t) is a generalised function that represents the tracer injection in time (in s^{-1}).

This analytical solution assumes that the tracer injection at the upper boundary occurs in a unit pulse input. In reality, a unit pulse input is never achievable. However, if a very short time for tracer injection at a constant rate is assumed (Eq. (2c)), this analytical solution produces satisfactory results (Lei et al., 2005).

$$\delta(t) = \frac{1}{t_i} \quad (2c)$$

where t_i is the time for tracer injection (in s^{-1}).

If conservation of the tracers in the flowing water is assumed, G_0 can be calculated as the integral area of the measured electrical conductivity or temperature curves with time (Eq. (3)). However, since both tracers are not fully conservative, this is only an approximation of the real value of G_0.

$$G_0 = \int_0^\infty G(x, t)dt \quad (3)$$

Therefore, in this generalised analytical solution, two parameters need to be determined to describe the transport of a solute or heat in the flow, i.e. D_H and U in the case of solute transport and D_T and U in the case of heat transport. They can be determined by fitting the analytical solution to solute or heat transport data obtained experimentally. For this purpose, solute transport data obtained with an electrical conductivity sensor and temperature data obtained with an infrared video camera from combined salt and thermal tracer experiments, described in Abrantes et al. (2018), were used.

3. Experimental methodology

3.1. Setup and simulated flows

The 3.00 m long by 0.15 m wide hydraulic flume (Fig. 1) was used to simulate flows in this study. The flume uses a water recirculation circuit with a 500 L reservoir, a pump and a flow control valve. The setup allows the manual adjustment of the bed slope. The flume has free inflow and outflow and so flow velocity and depth are controlled by the flow discharge, bed slope and bed surface roughness.

A total of 23 different flow conditions (velocities) were simulated, involving three bed surfaces (smooth acrylic sheet, rough sand board and synthetic grass carpet), three bed slopes (0.8, 4.4 and 13.2%) and different flow discharges (between 47 and 1239 ml s^{-1}), as summarised in Table 1. Smooth acrylic simulations were performed on the bed's smooth acrylic sheet. For the rough sand simulations, < 1.2 mm sieved sand particles were glued to an acrylic board that was fixed to the flume bed. For the synthetic grass simulations, an 8.5 mm thick synthetic grass carpet was fixed to the flume bed. Photographs, from above, of the three bed surfaces used in the experiments are shown in Fig. 2.

Table 1
Simulated flows.

Flow simulation	S (%)	Q (10^{-6} m^3 s^{-1})	h (10^{-3} m)	U_M (m s^{-1})
Smooth acrylic sheet				
Acrylic_1	0.8	650	9.12	0.475
Acrylic_2	0.8	856	11.06	0.516
Acrylic_3	0.8	1158	13.31	0.580
Acrylic_4	4.4	420	5.29	0.529
Acrylic_5	4.4	696	7.45	0.623
Acrylic_6	13.2	71	1.37	0.345
Acrylic_7	13.2	164	1.77	0.619
Acrylic_8	13.2	450	3.5	0.851
Rough sand board				
Sand_1	0.8	47	8.95	0.035
Sand_2	0.8	81	7.71	0.070
Sand_3	0.8	210	17.72	0.079
Sand_4	4.4	72	14.55	0.033
Sand_5	4.4	259	9.70	0.178
Sand_6	4.4	884	15.89	0.371
Synthetic grass carpet				
Grass_1	0.8	94	25.07	0.025
Grass_2	0.8	438	36.50	0.080
Grass_3	0.8	1067	45.60	0.156
Grass_4	4.4	75	n.a.m.	n.a.m.
Grass_5	4.4	549	17.68	0.207
Grass_6	4.4	1103	17.63	0.417
Grass_7	13.2	52	n.a.m.	n.a.m.
Grass_8	13.2	202	11.41	0.118
Grass_9	13.2	1239	17.92	0.461

S for slope; Q for discharge; h for flow depth; U_M for mean flow velocity from discharge/depth measurements; n.a.m. for not able to measure.

For each simulated flow, flow depth was measured using a point gauge (Fig. 1a) and flow discharge was measured at the flume outlet by the volumetric method.

3.2. Tracer techniques

Flow velocity was measured using salt and thermal tracer techniques. The two techniques were tested simultaneously in a double tracer consisting of salted-heated water (Fig. 1a). This was made by adding common table salt to tap water, in a ratio of 5 g of salt per litre of water (corresponding to an electrical conductivity of approximately 9000 μS cm^{-1}), and heating this solution in an electrical kettle to a temperature well above the average flow water temperature (71.3 ± 5.2 °C immediately before injecting the tracer into the flow). A volume of 10 ml of tracer per 100 ml s^{-1} of flow discharge was used in each flow velocity measurement. Salt concentration, temperature and volume of tracer were established in preliminary tests and shown to be appropriate, enabling the tracer to be detected in the flow by the two techniques. Any differences in density and viscosity between flow and tracer due to differences in salt concentration and temperature should be minimal and should not have a significant influence on the transport of the tracer in the flow. The tracer was injected manually into the flow in a quick movement, 2.1 m upslope of the channel outlet (Fig. 1b).

The movement of the tracer in the flow was detected with (Fig. 1): i) A CON-BTA conductivity sensor (from Vernier Software & Technology LLC, USA), with a temporal resolution of 0.2 s, an accuracy of ± 3%, at the mid-range of 0–2000 μS cm^{-1}; and ii) An Optris PI-160 infrared video camera (from Optris GmbH, Germany), with a temporal resolution of 0.01 s, a thermal resolution of 0.1 °C, an accuracy of ± 2%, at the spectral range of 7.5–13.0 μm. The conductivity sensor was placed in a spillway immediately in front of the channel outlet (Fig. 1a). The infrared camera was fixed to a metal structure 4 m above the flume, with the field of view (23° × 17°) covering 1.60 m of the flume length and the entire width of 0.15 m, providing thermal imaging of 156 × 13 pixels (Fig. 1b).

The tracer techniques were applied three times for each simulated flow.

3.3. Data analyses

Flow velocity was estimated following three different automatic methodologies, as schematised in Fig. 3: i) Velocities from the leading edge of the tracers (U_{LE}); ii) Velocities from the centroid of the tracers (U_C); and iii) Velocities from fitting the analytical solution of solute transport to data obtained from the tracers (U_{AS}). Estimated velocities from the three methodologies and two tracers were compared to mean flow velocity calculated using discharge/depth measurements, according Eq. (4):

$$U_M = \frac{Q}{h \times w} \quad (4)$$

where U_M is the mean flow velocity (m s^{-1}), Q is the flow discharge (m^3 s^{-1}), h is the flow depth (m) and w is the width of the hydraulic flume (m).

Hydraulic parameters for the different simulated flows are shown in Table 1.

Electrical conductivity and temperature data obtained with the tracer techniques were transformed in order to properly estimate flow velocities automatically. Firstly, threshold values of electrical conductivity and temperature were established to distinguish values associated with the tracer from values associated with the background flow. These threshold values corresponded to the maximum electrical conductivity and temperature measured in the 5 s before the injection of the tracer (EC_{MAX} and T_{MAX}), as schematised in Fig. 3a. A maximum value instead of a mean value was chosen as a threshold value to be more certain that only values associated with the tracer were identified

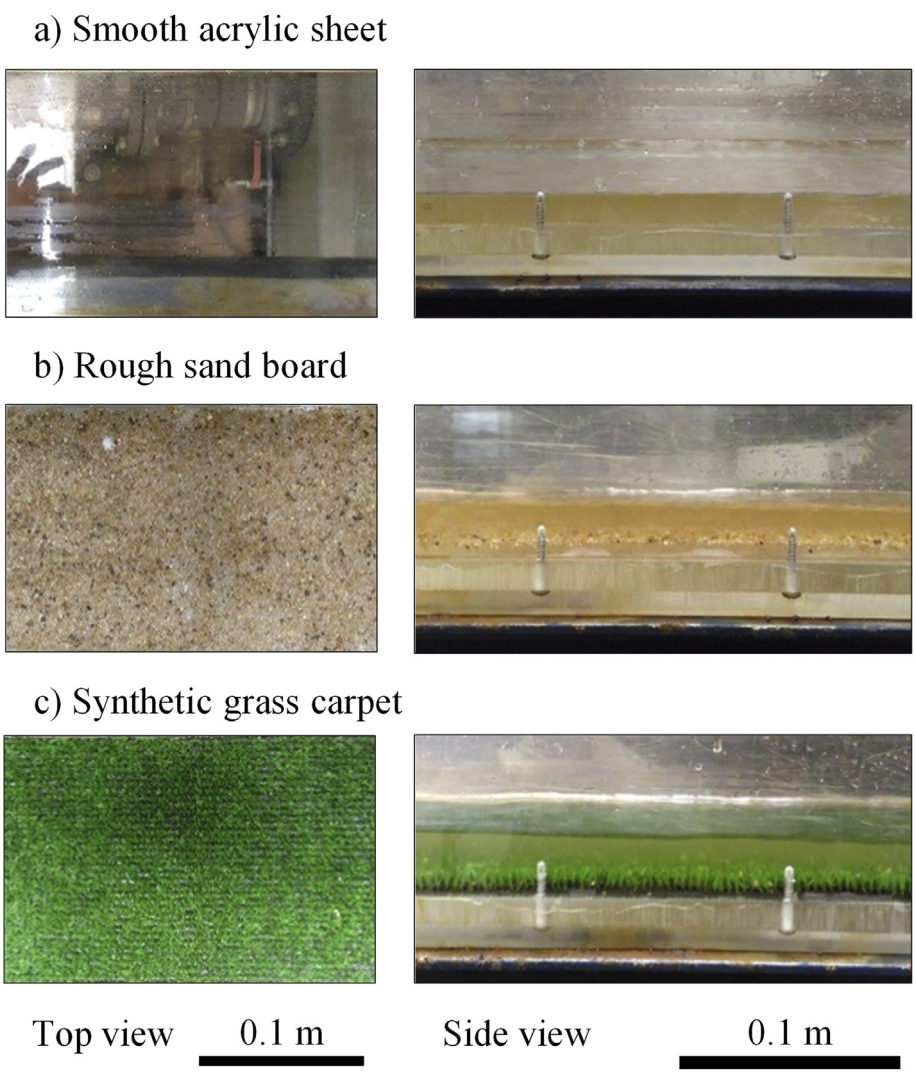

Fig. 2. Photographs of the three bed surfaces used in the experiments: a) Smooth acrylic sheet; b) Rough sand board; c) Synthetic grass carpet. View from above, without flowing water (left) and side view with flowing water (right).

automatically. These threshold values were subtracted from the corresponding electrical conductivity and temperature measured during the passage of tracer (Fig. 3b) and negative values were set to 0. Secondly, since absolute values of electrical conductivity and temperature were not important to estimate the flow velocity, they were normalised in order to compare the curves of solute and heat transport. This was done by dividing the electrical conductivity and temperature values by the respective concentration or temperature injected at the upper boundary. In the generalised form:

$$NG(x, t) = \frac{G(x, t)}{G(0, t)} = t_i \times \frac{G(x, t)}{G_0} \quad (5a)$$

where NG represents either the dimensionless normalised values of solute concentration (NC, proportional to the electrical conductivity, NEC) or the dimensionless normalised values of tracer temperature (NT).

Since the tracer was injected manually into the flow in a quick movement in a very short time (i.e. approximated to a unit pulse input), the time for tracer injection (t_i) was practically impossible to measure or estimate. Therefore, the normalised values were expressed as a ratio of the tracer injection time (Eq. (5b)), i.e. dimensionless values of electrical conductivity or temperature per second of tracer injection (NEC/t_i or NT/t_i in s^{-1}), as represented in Fig. 3c. This normalisation assumes a consistent tracer injection time throughout the experiments.

$$\frac{NG}{t_i}(x, t) = \frac{G(x, t)}{G_0} \quad (5b)$$

These normalised values (Eq. (5b)) can vary between 0 and ∞ (greatly depend on the tracer injection time) and the integral area of the normalised curves with time is equal to 1.

The leading edge (U_{LE}) and centroid (U_C) velocities of the tracers were calculated automatically, following procedure schematised in Fig. 3c. In the first case this was done by dividing the distance travelled from the injection of the tracer to the detection sections (2.1 m for the salt tracer and 0.5, 1.0, 1.5 and 2.0 m for the thermal tracer as schematised in Fig. 2b) by the time taken from the tracer injection to the first rise (i.e. first non-zero value) in the normalised electrical conductivity and temperature (t_{LE}). In the second case, the travelled distance was divided by the time taken for the centroid of the normalised electrical conductivity and temperature graphs to arrive (t_C), calculated as follows:

$$t_C = \frac{\sum_{t=0}^{\infty}\left(\frac{NG}{t_i}(x, t) \times t\right)}{\sum_{t=0}^{\infty}\frac{NG}{t_i}(x, t)} \quad (6)$$

For each flow condition, velocities from fitting the analytical solution (Eq. (2)) to salt and thermal tracers' data (U_{AS}) were determined by minimising the sum of squared errors between modelled and

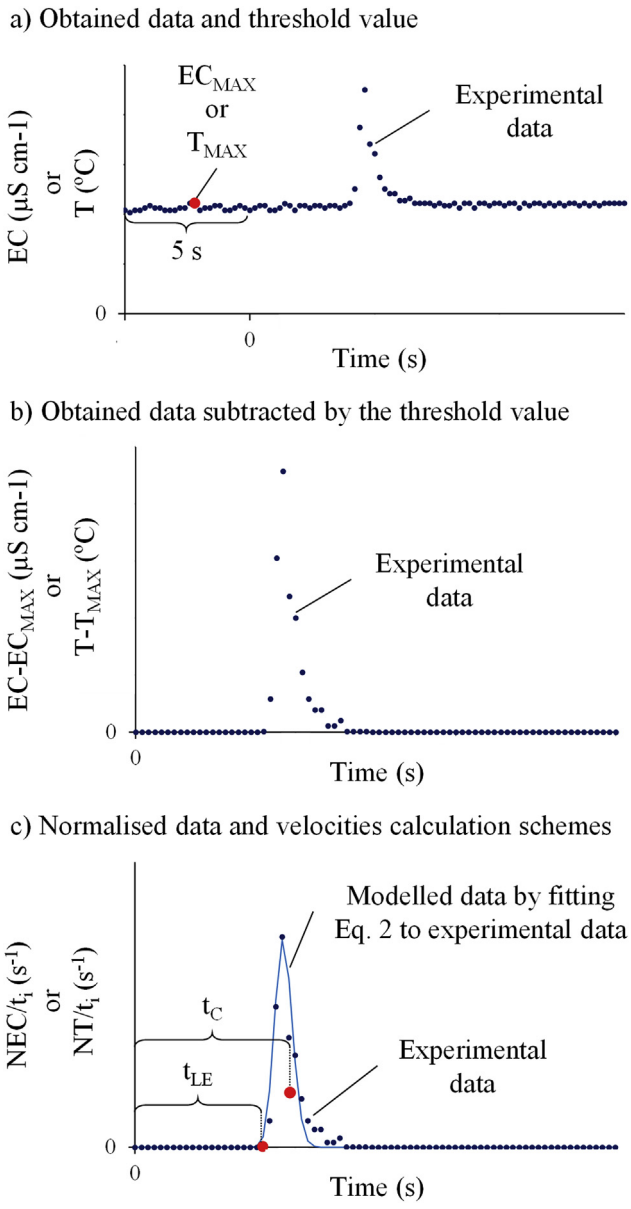

Fig. 3. Procedure used to calculate the velocity of the salt and thermal tracers: a) Data observed experimentally from measurements with the electrical conductivity sensor or the infrared video camera and identification of the threshold value (EC_{MAX} or T_{MAX}); b) Observed data subtracted by the threshold value; c) Data normalisation and identification of the time taken by the leading edge (t_{LE}) and centroid (t_C) of the tracers, as well as representation of the modelled data (solid line) fitted to the observed data (markers).

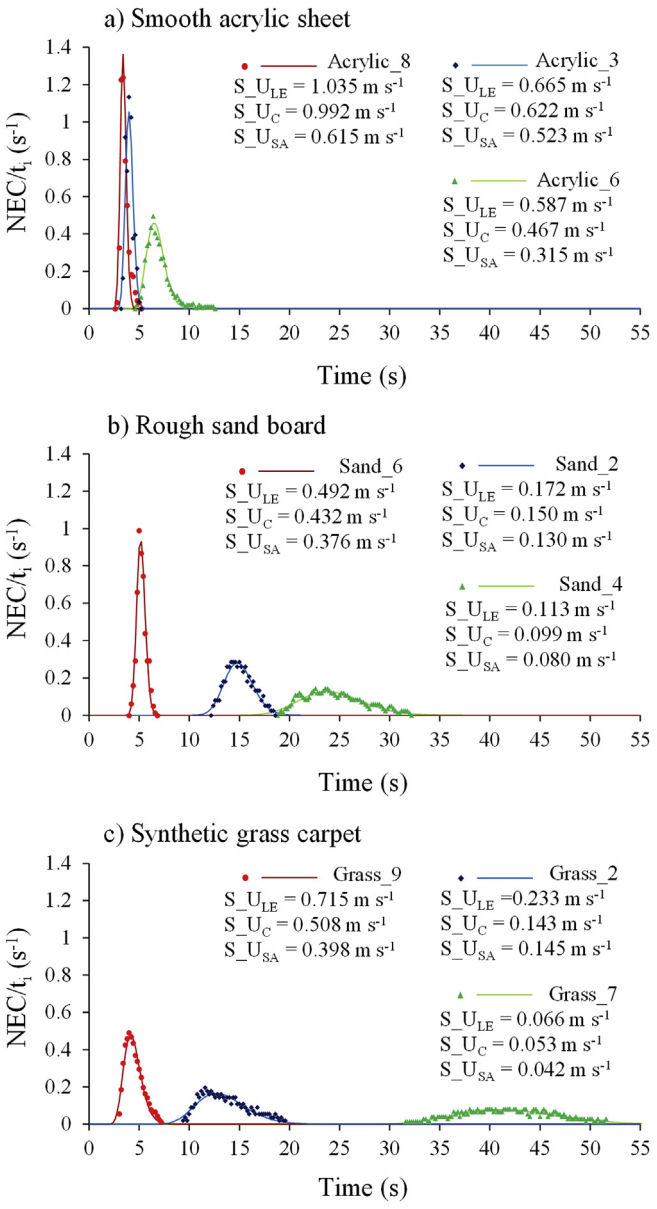

Fig. 4. Salt tracer leading edge velocity (U_{LE}) and centroid (U_C) velocity, and velocity estimated from fitting the analytical solution of solute transport to electric conductivity data (U_{AS}) for the three bed surfaces: a) Smooth acrylic sheet; b) Rough sand board; c) Synthetic grass carpet. For each bed surface, data observed 2.1 m from the tracer injection point (markers) and the corresponding fitted modelled curves (solid lines) of three simulated flows are shown. For each simulated flow, data from one repetition is shown.

experimentally observed data, as schematised in Fig. 3c. The hydrodynamic dispersion coefficient (D_H) and thermal dispersion coefficient (D_T) were also determined. The performance of the numerical method was evaluated using the determination coefficient (r^2) to compare modelled and experimentally observed data. One-way analysis of variance (one-way ANOVA) with post hoc Tukey-Kramer honestly significant difference (HSD) test at levels of significance of 0.05 and 0.01 was performed as a multiple comparison of r^2 values to ascertain if the performance of the numerical methodology differed significantly between tracer techniques, bed surfaces and measuring distances to tracer injection point.

4. Results and discussion

Graphs of experimentally observed electrical conductivity and temperature data (markers) and the corresponding fitted analytical solute and heat transport curves (smooth solid curves) are shown in Figs. 4 and 5, respectively; results of three simulated flows for the salt tracer and two simulated flows for the thermal tracer are shown. Velocity results for all bed surfaces and simulated flows, comprising a total of 23 different flow conditions, are shown in Table 2 (salt tracer) and Table 3 (thermal tracers). Salt tracer velocities (Fig. 4 and Table 2) were measured 2.1 m from the tracer injection point and thermal tracer velocities were measured 0.5, 1.0, 1.5 and 2.0 m from the tracer injection point (Fig. 5 and Table 3).

From Figs. 4 and 5 it can be seen that, in general, the analytical

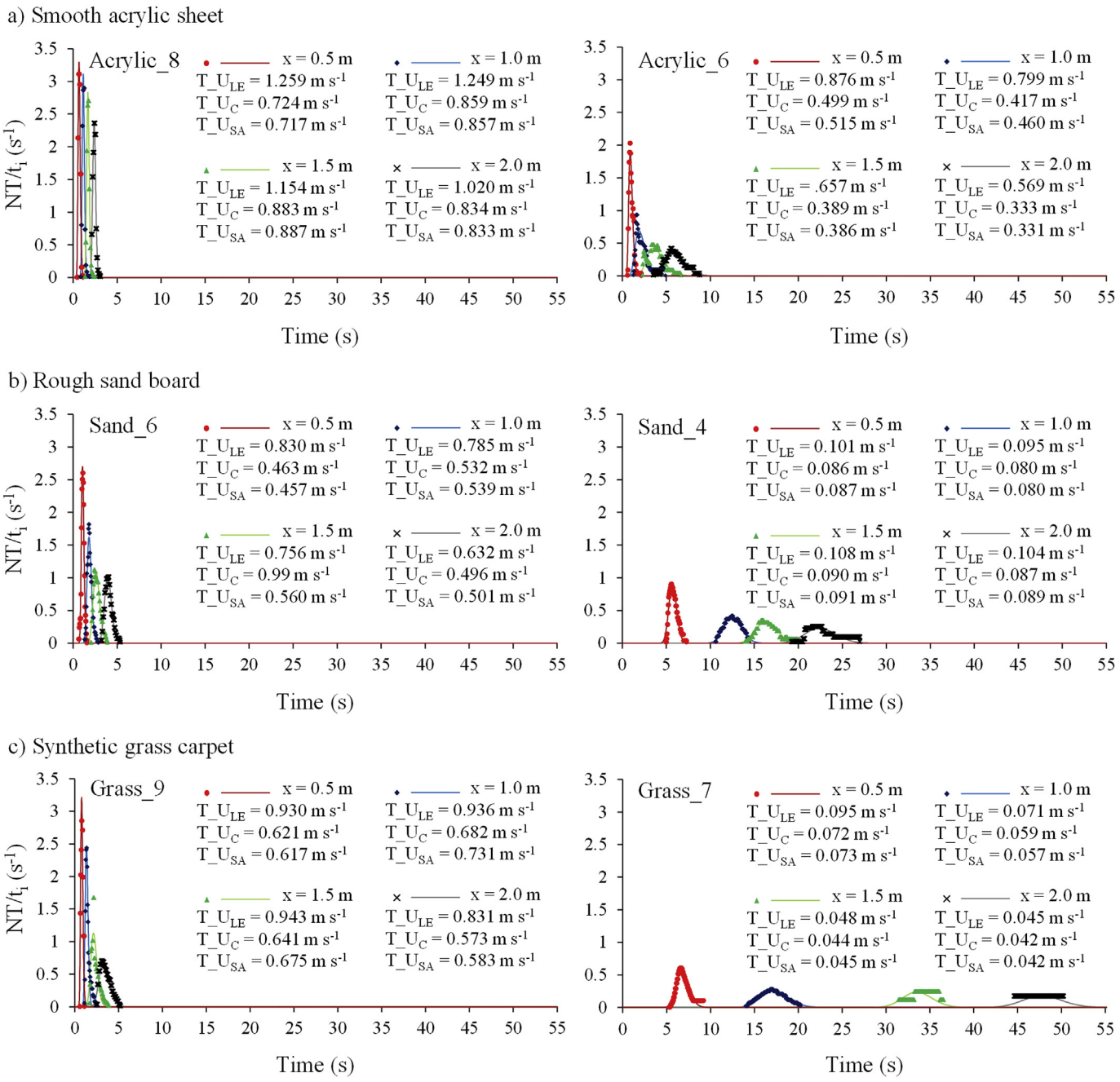

Fig. 5. Thermal tracer leading edge (U_{LE}) and centroid (U_C) velocities, as well as velocities estimated from fitting the analytical solution of solute transport to temperature data (U_{AS}) for the three bed surfaces: a) Smooth acrylic sheet; b) Rough sand board; and c) Synthetic grass carpet. For each bed surface, data observed 0.5, 1.0, 1.5 and 2.0 m from the tracer injection point (markers) and the corresponding fitted modelled curves (solid lines) of two simulated flows are shown. For each simulated flow, data from one repetition is shown.

solution of the solute and heat transport successfully modelled the electrical conductivity and temperature data observed in the salt and thermal tracer experiments. The modelled data simulated the peaks and the increasing and decreasing curves of the observed data well. As expected, due to diffusion effects the observed and modelled temperature peaks (Fig. 5) decreased with increasing distance from the tracer injection point.

Determination coefficients (r^2) comparing modelled and experimentally observed data are shown in Fig. 6; thermal tracer results correspond to temperature measurements at 0.5, 1.0, 1.5 and 2.0 m from the tracer injection point and salt tracer results correspond to electrical conductivity measurements at 2.1 m from the tracer injection point. For all simulated flows, on average, r^2 values higher than 0.85 were obtained. Generally, the solute transport model better represented the electrical conductivity data observed with the salt tracer than the temperature data observed with the thermal tracer. Also, the r^2 of the temperature data decreased with increasing distance from the tracer injection point. In previous studies of solute transport data (Lei et al., 2005, 2010; 2013; Shi et al., 2012) no clear relation has been observed between the model performance and the distance from the tracer injection point. As stated before, thermal tracers have been shown to be less conservative than salt tracers (Abrantes et al., 2018; Schuetz et al., 2012), and therefore it is expected a lower performance of the heat transport model than the solute transport model. In any case, differences in the model performance between both tracer techniques and between different distances from the tracer injection point were never

Table 2
Salt tracer velocities measured 2.1 m from the tracer injection point. Values are average of three repetitions.

Salt tracer velocities (m s^{-1})			
Flow simulation	U_{LE}	U_C	U_{AS}
Acrylic_1	0.596	0.540	0.453
Acrylic_2	0.639	0.547	0.481
Acrylic_3	0.637	0.597	0.506
Acrylic_4	0.595	0.552	0.461
Acrylic_5	0.717	0.649	0.534
Acrylic_6	0.591	0.460	0.310
Acrylic_7	0.725	0.573	0.401
Acrylic_8	0.901	0.945	0.567
Sand_1	0.080	0.106	0.090
Sand_2	0.138	0.108	0.129
Sand_3	0.156	0.143	0.087
Sand_4	0.122	0.095	0.078
Sand_5	0.317	0.252	0.213
Sand_6	0.538	0.441	0.381
Grass_1	0.109	0.052	0.043
Grass_2	0.225	0.151	0.144
Grass_3	0.307	0.194	0.214
Grass_4	0.072	0.058	0.045
Grass_5	0.472	0.284	0.248
Grass_6	0.564	0.371	0.334
Grass_7	0.062	0.055	0.043
Grass_8	0.210	0.147	0.118
Grass_9	0.752	0.545	0.425

U_{LE} and U_C for salt tracer leading edge and centroid velocities; U_{AS} for velocities estimated from fitting the analytical solution of solute transport to electrical conductivity data.

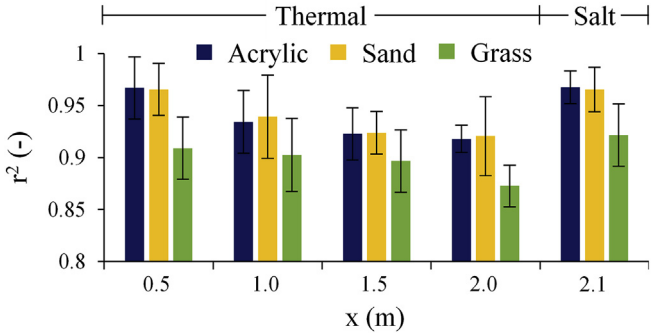

Fig. 6. Determination coefficient (r^2) comparing modelled and experimentally observed data. Temperature data from thermal tracer measurements at 0.5, 1.0, 1.5 and 2.0 m from the tracer injection point and electrical conductivity data from salt tracer measurements at 2.1 m from the tracer injection point.

significant.

The performance of the solute and heat transport models was not influenced by the flow velocity or bed slope; no clear relation was observed between them, as shown in previous studies for solute transport in Lei et al. (2005, 2010, 2013), Rahma et al. (2013) and Shi et al. (2012). However, for both tracers, flow simulations on the synthetic grass carpet showed lower values of r^2 than those on the smooth acrylic sheet and rough sand board. It was expected that modelling the movement of a tracer in the flow over a rough element such as the synthetic grass carpet would be a more complex task due to the higher flow disturbances, higher diffusion, and higher exchanges of tracer between the flow and the rough element. In any case, differences in the model performance between the different simulated flows, bed surfaces and distances from the tracer injection point were never significant. While this was reported before in Rahma et al. (2013) for the electrical

Table 3
Thermal tracer velocities measured 0.5, 1.0, 1.5 and 2.0 m from the tracer injection point. Values are average of three repetitions.

Thermal tracer velocities (m s^{-1})												
Flow simulation	U_{LE}				U_C				U_{AS}			
	x (m)											
	0.5	1.0	1.5	2.0	0.5	1.0	1.5	2.0	0.5	1.0	1.5	2.0
Acrylic_1	0.763	0.707	0.635	0.601	0.660	0.617	0.596	0.595	0.453	0.456	0.387	0.414
Acrylic_2	0.787	0.813	0.762	0.695	0.544	0.714	0.698	0.670	0.429	0.443	0.489	0.456
Acrylic_3	0.843	0.867	0.839	0.754	0.760	0.763	0.757	0.756	0.489	0.577	0.588	0.554
Acrylic_4	0.846	0.803	0.695	0.638	0.604	0.647	0.642	0.625	0.524	0.419	0.387	0.418
Acrylic_5	0.948	0.983	0.931	0.819	0.750	0.793	0.759	0.774	0.555	0.683	0.546	0.523
Acrylic_6	0.872	0.795	0.654	0.566	0.507	0.599	0.372	0.370	0.415	0.372	0.311	0.326
Acrylic_7	1.214	1.177	1.001	0.769	0.912	0.721	0.753	0.669	0.647	0.668	0.502	0.398
Acrylic_8	1.265	1.256	1.160	1.025	0.937	0.827	0.843	0.924	0.581	0.731	0.806	0.700
Sand_1	0.125	0.125	0.119	0.091	0.06	0.079	0.079	0.079	0.079	0.079	0.077	0.056
Sand_2	0.138	0.132	0.122	0.115	0.099	0.117	0.115	0.118	0.100	0.097	0.094	0.089
Sand_3	0.304	0.203	0.181	0.170	0.334	0.259	0.208	0.162	0.162	0.114	0.093	0.104
Sand_4	0.101	0.094	0.107	0.104	0.115	0.11	0.105	0.100	0.083	0.076	0.087	0.084
Sand_5	0.576	0.463	0.420	0.328	0.431	0.308	0.295	0.263	0.334	0.272	0.245	0.184
Sand_6	0.830	0.785	0.756	0.632	0.598	0.568	0.567	0.519	0.487	0.459	0.455	0.470
Grass_1	0.128	0.111	0.091	0.083	0.048	0.061	0.074	0.087	0.078	0.066	0.057	0.052
Grass_2	0.418	0.267	0.229	0.190	0.231	0.175	0.198	0.177	0.268	0.186	0.184	0.120
Grass_3	0.379	0.372	0.357	0.334	0.319	0.336	0.283	0.293	0.272	0.266	0.257	0.229
Grass_4	0.092	0.060	0.044	0.043	0.057	0.038	0.030	0.048	0.051	0.034	0.025	0.023
Grass_5	0.682	0.571	0.486	0.427	0.477	0.292	0.323	0.305	0.429	0.350	0.288	0.253
Grass_6	0.690	0.698	0.694	0.681	0.861	0.522	0.516	0.519	0.515	0.529	0.522	0.487
Grass_7	0.094	0.071	0.047	0.045	0.061	0.051	0.036	0.035	0.069	0.054	0.039	0.038
Grass_8	0.288	0.228	0.140	0.173	0.154	0.111	0.109	0.144	0.180	0.132	0.090	0.110
Grass_9	0.923	0.929	0.936	0.825	0.845	0.744	0.503	0.688	0.539	0.631	0.586	0.508

U_{LE} and U_C for thermal tracer leading edge and centroid velocities; U_{AS} for velocities estimated from fitting the analytical solution of solute transport to temperature data; x distance from tracer injection point.

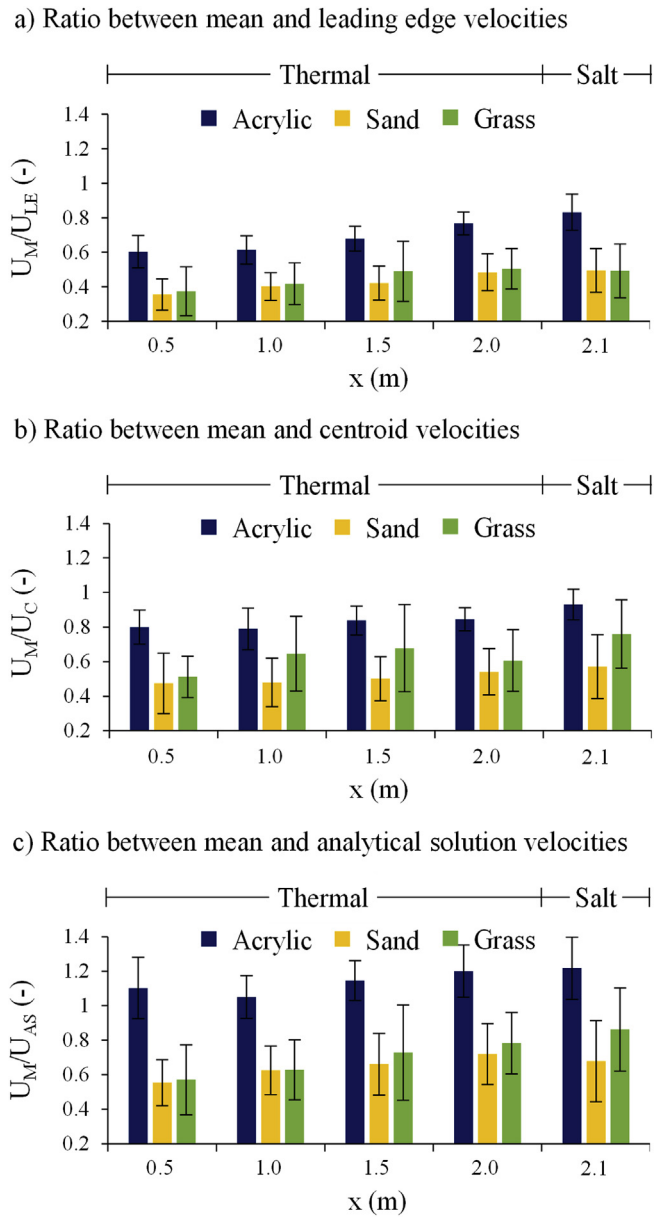

Fig. 7. Ratio between mean flow velocity (U_M) calculated from discharge/depth measurements and: a) Leading edge velocity (U_{LE}); b) Centroid velocity (U_C); c) Velocity from fitting the analytical solution of solute transport to observed data (U_{AS}). Data from thermal tracer measurements at 0.5, 1.0, 1.5 and 2.0 m from the tracer injection point and salt tracer measurements at 2.1 m from the tracer injection point.

conductivity data (salt tracer), it was a novelty for the temperature data (thermal tracer).

Ratios between the mean flow velocity (U_M) calculated from discharge/depth measurements and the leading edge (U_{LE}), centroid (U_C) and analytical solution (U_{AS}) velocities for both tracers are shown in Fig. 7; thermal tracer results correspond to temperature measurements at 0.5, 1.0, 1.5 and 2.0 m from the tracer injection point and salt tracer results correspond to electrical conductivity measurements at 2.1 m from the tracer injection point.

For both tracers, the leading edge (Fig. 7a) and centroid (Fig. 7b) velocities were higher than mean flow velocity, with ratios lower than 1, as observed in Abrantes et al. (2018). The leading edge had the higher velocity values, and therefore lower ratios, varying between 0.23 and 0.94 for the salt tracer and between 0.30 and 0.83 for the thermal tracer (for measurements at 2.0 m from the tracer injection point), with average values of 0.62 and 0.60, respectively. As stated before, the leading edge is regarded as the surface flow velocity, which corresponds to the maximum (or near maximum) value of the flow velocity profile. These values are in accordance with Horton's theoretical value of 0.67 (Horton et al., 1934) and with the range of approximately 0.2–0.9 found in the previous studies of Dunkerley (2001), Emmett (1970), Li and Abrahams (1997), Li et al. (1996), Planchon et al. (2005) and Zhang et al. (2010). The centroid velocity, meanwhile, is regarded as the theoretical mean value of the flow velocity profile, if conservation of the tracer in the flow is assumed. However, since none of the tracers exhibited absolute conservation during the experiments, centroid velocities were higher than mean flow velocity. For the centroid velocities the corresponding ratios were 0.33–1.13 for the salt tracer and 0.33–0.93 for the thermal tracer, with average values of 0.77 and 0.68, respectively. The lower value of 0.33 came below the range of 0.7–0.9 observed by Li et al. (1996) and 0.6–1.0 observed by Planchon et al. (2005).

Velocities from fitting the analytical solutions of solute and heat transport to data obtained from both tracers (U_{AS}) gave the highest ratios (Fig. 7c), with values ranging between 0.39 and 1.54 for the salt tracer and between 0.39 and 1.55 for the thermal tracer (for measurements at 2.0 m from the tracer injection point), with average values of 0.95 and 0.92, respectively. Therefore, on average, velocities from the numerical methods, were the ones that better predicted the mean flow velocity calculated from discharge/depth measurements.

It should be noted that the ratios between the mean flow velocity and tracer velocities are the result of a very complex relationship between the shape of the flow velocity profile and the flow characteristics (e.g. velocity, depth, Reynolds number, Froude number) and the bed surface characteristics (e.g. roughness, slope), as shown in Abrantes et al. (2018), Dunkerley (2001), Emmett (1970), Li and Abrahams (1997), Li et al. (1996), Planchon et al. (2005) and Zhang et al. (2010). In the present study, a strong positive correlation was found between these ratios and the flow regime. An increase in Reynolds and Froude numbers increases flow turbulence and flow speed, which results in a better mixing of the flow, and a less steep velocity profile, approaching the flow velocity profile mean and maximum values. Therefore, ratios between the mean flow velocity and tracer velocities closer to 1. In general, these ratios varied directly with flow velocity and slope and varied inversely with flow depth and bed roughness. In Fig. 7, perceptible differences can be seen between the smooth acrylic sheet, the rough sand board and the synthetic grass carpet, with the two latter presenting lower values. Flow velocity estimation from tracers involves a large amount of uncertainty and caution is required when using these measurements. A more detailed analysis on the results of these tracer experiments and on the variation of these ratios with the flow and bed surface characteristics can be seen in Abrantes et al. (2018).

Thermal tracer velocities decreased with increasing distance from the tracer injection point, as can be seen by the higher values in Fig. 7. This effect was observed in Abrantes et al. (2018) for the leading edge (Fig. 7a) and centroid (Fig. 7b) velocities and it can be related to two aspects. On the one hand, higher velocities closer to the tracer injection point can be caused by the disturbance of the tracer injection itself, even with the minimum distance of 0.5 m from the tracer injection point. On the other hand, the non-conservative aspect of the thermal tracer results in a decrease of tracer temperature as the distance from the tracer addition point increases, and therefore the tracer temperature slowly dissipates in the background water temperature. This effect had more impact on the leading edge than on the centroid because temperature dissipation occurs first in the interface between the tracer and the flow. At a lesser extent, the thermal analytical solution velocities (U_{AS}) also decreased with increasing distance to the tracer injection point (Fig. 7c). On the contrary, in Lei et al. (2005, 2010, 2013), Rahma et al. (2013) and Shi et al. (2012) a slight increase of the numerically determined velocities with increasing distance from the tracer injection point was observed with salt tracer measurements. In these studies, the

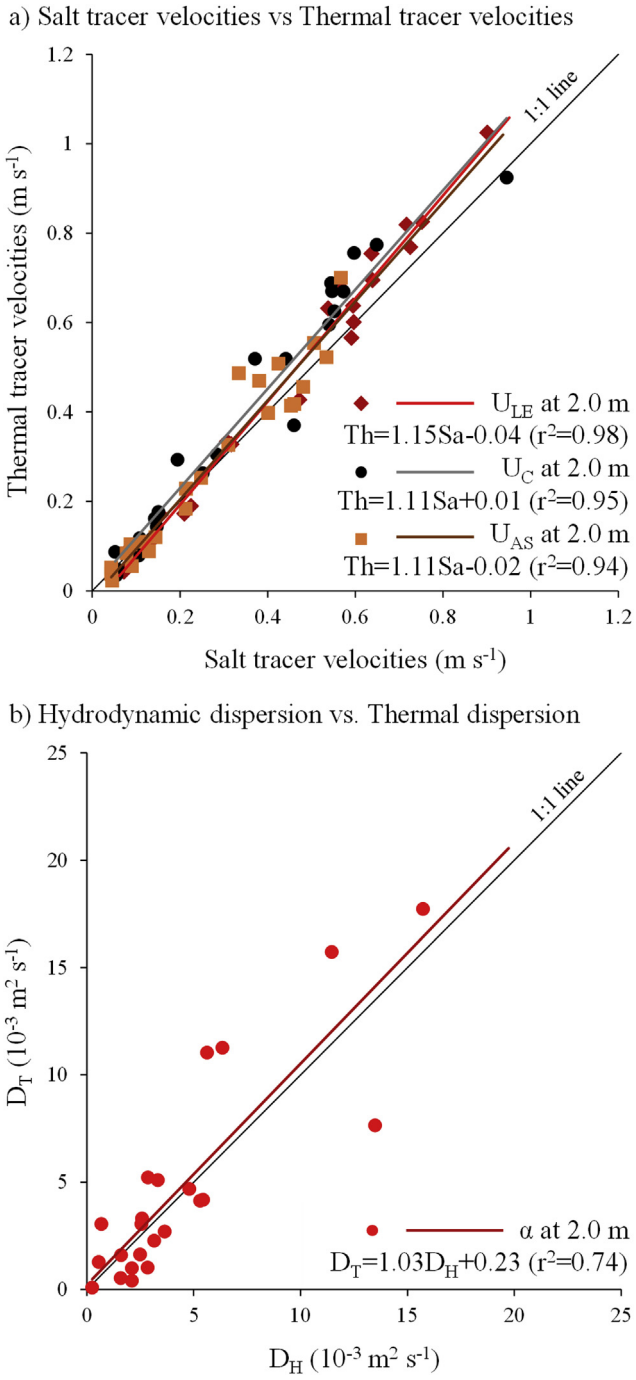

Fig. 8. Comparison between salt and thermal tracer results: a) Leading edge (U_{LE}), centroid (U_C) and analytical solution (U_{AS}) velocities; and b) Hydrodynamic dispersion (D_H) against thermal dispersion (D_T). Salt and thermal tracer results from measurements taken 2.1 and 2.0 m, respectively, from the tracer injection point.

flow was considered to still be accelerating as it passed through the measuring points. However, the main difference is that salt tracer measurements were conducted. As stated before, salt tracer was found to be more conservative than thermal tracer and the transport of salt has shown higher stability with increasing distance from the tracer injection point than the heat transport. Therefore, the accuracy of the flow velocity measurements seem to depend more on the volume and temperature of the thermal tracer (i.e. lower conservation may require a higher volume and/or temperature of the thermal tracer) than on the volume and concentration of the salt tracer (i.e. higher conservation may require a lower volume and/or concentration of the salt tracer).

Comparison between salt and thermal tracer velocities and between hydrodynamic and thermal dispersion coefficients is shown in Fig. 8; results of temperature measurements at 2.0 m from the tracer injection point are shown to make comparison possible with electrical conductivity measurements at 2.1 m from the tracer injection point. The thermal and salt tracer techniques yielded very similar results with a good correlation with one another (r^2 values higher than 0.94 in Fig. 8a). Generally, the thermal tracer resulted in slightly higher velocities than the salt tracer, with differences increasing with the flow velocity. Even so, differences between both tracers were never significant. A similar relationship between salt and thermal tracer techniques was noted in Abrantes et al. (2018) and Schuetz et al. (2012). Differences between the thermal and salt tracing were very similar for the three tracer velocities (i.e. leading edge, centroid and analytical solution), as can be seen by the linear regressions in Fig. 8a. In turn, differences between tracer techniques varied with the bed surface. On average, for the smooth acrylic sheet simulations the thermal tracer leading edge, centroid and analytical solution velocities were 8, 11 and 2% higher, respectively. For the rough sand board, the thermal tracer yielded 2 and 4% higher leading edge and centroid velocities, but 5% lower analytical solution velocities. For the synthetic grass carpet, the thermal tracer leading edge velocities were 11% lower, but the centroid and analytical solution velocities were 17 and 1% higher.

The correlation between hydrodynamic and thermal dispersion coefficients was not as marked as that between the tracers' velocities, as can be seen from the r^2 value of 0.74 in Fig. 8b. On average, the thermal dispersion was higher than the hydrodynamic dispersion. This difference between dispersion coefficients can be explained. Both dispersion coefficients contain a component of pure diffusion (i.e. mass diffusion for solute transport and thermal diffusion for heat transport) and a component of advection (i.e. hydrodynamic dispersivity for solute transport and thermal dispersivity for heat transport). In the previous studies of de Marsily (1986), Rau et al. (2012) and Vandenbohede et al. (2009) it is suggested that while usually the hydrodynamic and thermal dispersivity coefficients are approximately equal, the thermal diffusion coefficient can be up to orders of magnitude greater than the mass diffusion coefficient. Therefore, the thermal dispersion coefficient can be approximately equal up to orders of magnitude greater than the hydrodynamic dispersion coefficient. This difference depends on the type of flow. For advection dominated flows, such as the shallow flows simulated in this study with high flow rates, the effect of the mechanical advection greatly exceeds that of the molecular diffusion and the effect of pure mass and thermal diffusion is minimal. Therefore, thermal dispersion was only 17% higher than hydrodynamic dispersion. As a comparison, in the study of de Marsily (1986) of solute and heat transport by diffusion dominated flows in porous media, thermal dispersion coefficients up to approximately 500 times greater than hydrodynamic dispersion coefficients were observed. The higher thermal diffusivity ultimately explains the lower conservation of the thermal tracer than the salt tracer, as observed in Abrantes et al. (2018) and Schuetz et al. (2012).

5. Conclusions

A numerical methodology to estimate shallow flow velocity combining temperature data from thermal tracer measurements and an advection-dispersion heat transport model was tested. This methodology was compared to an identical methodology combining an advection-dispersion solute transport model with electrical conductivity data from salt tracer measurements. It can be concluded the proposed methodology can be used to estimate shallow flow velocity. The analytical solution of heat transport fitted the experimentally measured temperature data well under different shallow flow conditions, i.e. different flow discharges, bed slopes, bed surfaces. In fact, results from the numerical methodology predicted the mean flow velocity calculated

from discharge/depth measurements better than other more traditional and well-established methodologies, such as measuring the leading edge and centroid of the tracer.

Differences were observed between salt and thermal tracer velocities and between hydrodynamic and thermal dispersion coefficients. These differences result from the lower conservative aspect of the thermal tracer than the salt tracer, which ultimately can be explained by the higher thermal diffusion than the mass diffusion. This results in thermal tracer velocities less accurate and less stable than the salt tracer velocities. However, it should be noted that for this study's shallow flows and small measuring section, differences between both tracers were never significant. Also, some of these differences can also be explained due to some method errors, such as errors that occur due to differences in the response times and in the measurement temporal frequency between the infrared camera (thermal tracer) and the electrical conductivity sensor (salt tracer).

Velocity estimation from tracers in hydrologic research (e.g. soil erosion and solute transport studies) involves a large amount of uncertainty and caution is required when using these measurements, especially in the field. Tracking the movement of a thermal tracer in flowing water using an infrared camera has the advantage of measuring space-averaged flow velocity, which can greatly vary in space and time. For salt tracers this can only be achieved by installing multiple sensors, which can ultimately cause higher disturbance to the actual flow velocity. In this sense, the tested methodology using a thermal tracer can be a useful tool in such research areas. Further studies are therefore required to investigate performance of the numerical methodology in the presence of different hydrological processes (e.g. presence of sediments in the flow). Also, to achieve the best performance of the numerical methodology, further tests should be conducted using different volumes of tracer at different temperatures.

Acknowledgements

This work was supported by FCT, Portugal, and FEDER through the Doctoral grant SFRH/BD/103300/2014 of João Abrantes, the Project HIRT - Modelling surface hydrologic processes based on infrared thermography at local and field scales (PTDC/ECM-HID/4259/2014 – POCI-01-0145-FEDER-016668) coordinated by João Pedroso de Lima, and the Strategic project UID/MAR/04292/2013 granted to MARE, Portugal, and by CNPq, Brazil, through the Post-doctoral grants 451227/2016-6 of Rodrigo Moruzzi and 206872/2014-3 of Alexandre Silveira.

Appendix A. Supplementary data

Supplementary data to this article can be found online at https://doi.org/10.1016/j.pce.2018.12.005.

References

Abrahams, A.D., Parsons, A.J., Luk, S.-H., 1986. Field measurement of the velocity of overland flow using dye tracing. Earth Surf. Process. Landforms 11 (6), 653–657. https://doi.org/10.1002/esp.3290110608.

Abrantes, J.R.C.B., Moruzzi, R.B., Silveira, A., de Lima, J.L.M.P., 2018. Comparison of thermal, salt and dye tracing to estimate shallow flow velocities: novel triple tracer approach. J. Hydrol. 557, 362–377. https://doi.org/10.1016/j.jhydrol.2017.12.048.

Ban, Y., Lei, T., Liu, Z., Chen, C., 2016. Comparison of rill flow velocity over frozen and thawed slopes with electrolyte tracer method. J. Hydrol. 534, 630–637. https://doi.org/10.1016/j.jhydrol.2016.01.028.

Calkins, D., Dunne, T., 1970. A salt tracing method for measuring channel velocities in small mountain streams. J. Hydrol. 11 (4), 379–392. https://doi.org/10.1016/0022-1694(70)90003-X.

Chen, C., Ban, Y., Wang, X., Lei, T., 2017. Measuring flow velocity on frozen and non-frozen slopes of black soil through leading edge method. Int. Soil Water Conserv. Res. 5 (3), 180–189. https://doi.org/10.1016/j.iswcr.2017.02.004.

Comina, C., Lasagna, M., De Luca, D.A., Sambuelli, L., 2014. Geophysical methods to support correct water sampling locations for salt dilution gauging. Hydrol. Earth Syst. Sci. 18 (8), 3195–3203. https://doi.org/10.5194/hess-18-3195-2014.

Comiti, F., Mao, L., Wilcox, A., Wohl, E.E., Lenzi, M.A., 2007. Field-derived relationships for flow velocity and resistance in high-gradient streams. J. Hydrol. 340 (1–2), 48–62. https://doi.org/10.1016/j.jhydrol.2007.03.021.

Day, T.J., 1977. Observed mixing lengths in mountain streams. J. Hydrol. 35 (1–2), 125–136. https://doi.org/10.1016/0022-1694(77)90081-6.

de Lima, C.A., de Lima, J.L.M.P., Montenegro, A.A.A., Abrantes, J.R.C.B., Mujtaba, B., Silveira, A., 2018. Comparative evaluation of factors influencing seed displacement over the soil of nonconventional perennial crops: moringa (Moringa oleifera Lam.) and neem (Azadirachta indica A. Juss.). Soil Sci. https://doi.org/10.1097/SS.0000000000000219.

de Lima, J.L.M.P., Abrantes, J.R.C.B., 2014. Using a thermal tracer to estimate overland and rill flow velocities. Earth Surf. Process. Landforms 39 (10), 1293–1300. https://doi.org/10.1002/esp.3523.

de Lima, R.L.P., Abrantes, J.R.C.B., de Lima, J.L.M.P., de Lima, M.I.P., 2015. Using thermal tracers to estimate flow velocities of shallow flows: laboratory and field experiments. J. Hydrol. Hydromechanics 63 (3), 255–262. https://doi.org/10.1515/johh-2015-0028.

de Marsily, G., 1986. Quantitative Hydrogeology: Groundwater Hydrology for Engineers, first ed. Academic Press, San Diego, California, USA.

Dunkerley, D., 2001. Estimating the mean speed of laminar overland flow using dye injection-uncertainty on rough surfaces. Earth Surf. Process. Landforms 26 (4), 363–374. https://doi.org/10.1002/esp.185.

Dunkerley, D., 2003. An optical tachometer for short-path measurement of flow speeds in shallow overland flows: improved alternative to dye timing. Earth Surf. Process. Landforms 28 (7), 777–786. https://doi.org/10.1002/esp.468.

Emmett, W.W., 1970. The Hydraulics of Overland Flow on Hillslopes. Geological Survey Professional Paper 662-A. U.S. Government Printing Office, Washington, D.C., USA.

Flury, M., Flühler, H., 1993. Brilliant Blue FCF as a dye tracer for solute transport studies: a toxicological overview. J. Environ. Qual. 23 (5), 1108–1112. https://doi.org/10.2134/jeq1994.00472425002300050037x.

Holden, J., Kirkby, M.J., Lane, S.N., Milledge, D.G., Brookes, C.J., Holden, V., McDonald, A.T., 2008. Overland flow velocity and roughness properties in peatlands. Water Resour. Res. 44 (6), W06415. https://doi.org/10.1029/2007WR006052.

Horton, R.E., Leach, H.R., Vliet, V.R., 1934. Laminar sheet flow. Eos T. Am. Geophys. Un. 15 (2), 393–404. https://doi.org/10.1029/TR015i002p00393.

Huang, Y., Chen, X., Li, F., Zhang, J., Lei, T., Li, J., Chen, P., Wang, X., 2018. Velocity of water flow along saturated loess slopes under erosion effects. J. Hydrol. 561, 304–311. https://doi.org/10.1016/j.jhydrol.2018.03.070.

Lei, T., Chuo, R., Zhao, J., Shi, X., Liu, L., 2010. An improved method for shallow water flow velocity measurement with practical electrolyte inputs. J. Hydrol. 390 (1–2), 45–56. https://doi.org/10.1016/j.jhydrol.2010.06.029.

Lei, T., Xia, W., Zhao, J., Liu, Z., Zhang, Q., 2005. Method for measuring velocity of shallow water flow for soil erosion with an electrolyte tracer. J. Hydrol. 301 (1–4), 139–145. https://doi.org/10.1016/j.jhydrol.2004.06.025.

Lei, T., Yan, Y., Shi, X., Chuo, R., Zhao, J., 2013. Measuring velocity of water flow within a gravel layer using an electrolyte tracer method with a Pulse Boundary model. J. Hydrol. 500, 37–44. https://doi.org/10.1016/j.jhydrol.2013.07.025.

Li, G., Abrahams, A.D., 1997. Effect of saltating sediment load on the determination of the mean velocity of overland flow. Water Resour. Res. 33 (2), 341–347. https://doi.org/10.1029/96WR02937.

Li, G., Abrahams, A.D., Atkinson, J.F., 1996. Correction factors in the determination of mean velocity of overland flow. Earth Surf. Process. Landforms 21 (6), 509–515. https://doi.org/10.1002/SICI1096-983719960621:6<509::AID-ESP613>3.0.CO;2-Z.

Planchon, O., Silvera, N., Gimenez, R., Favis-Mortlock, D., Wainwright, J., Le Bissonnais, Y., Govers, G., 2005. An automated salt-tracing gauge for flow-velocity measurement. Earth Surf. Process. Landforms 30 (7), 833–844. https://doi.org/10.1002/esp.1194.

Rahma, A.E., Lei, T., Shi, X., Dong, Y., Zhou, S., Zhao, J., 2013. Measuring flow velocity under straw mulch using the improved electrolyte tracer method. J. Hydrol. 495, 121–125. https://doi.org/10.1016/j.jhydrol.2013.04.049.

Rau, G.C., Andersen, M.S., Acworth, R.I., 2012. Experimental investigation of the thermal dispersivity term and its significance in the heat transport equation for flow in sediments. Water Resour. Res. 48 (3), W03511. https://doi.org/10.1029/2011WR011038.

Schuetz, T., Weiler, M., Lange, J., Stoelzle, M., 2012. Two-dimensional assessment of solute transport in shallow waters with thermal imaging and heated water. Adv. Water Resour. 43, 67–75. https://doi.org/10.1016/j.advwatres.2012.03.013.

Shi, X., Lei, T., Yan, Y., Zhang, F., 2016. Determination and impact factor analysis of hydrodynamic dispersion coefficient within a gravel layer using an electrolyte tracer method. Int. Soil Water Conserv. Res. 4 (2), 87–92. https://doi.org/10.1016/j.iswcr.2016.05.001.

Shi, X., Zhang, F., Lei, T., Chuo, R., Zhou, S., Yan, Y., 2012. Measuring shallow water flow velocity with virtual boundary condition signal in the electrolyte tracer method. J. Hydrol. 452–453, 172–179. https://doi.org/10.1016/j.jhydrol.2012.05.046.

Tatard, L., Planchon, O., Wainwright, J., Nord, G., Favis-Mortlock, D., Silvera, N., Ribolzi, O., Esteves, M., Huang, C.H., 2008. Measurement and modelling of high-resolution flow-velocity data under simulated rainfall on a low-slope sandy soil. J. Hydrol. 348 (1–2), 1–12. https://doi.org/10.1016/j.jhydrol.2007.07.016.

Tauro, F., Grimaldi, S., 2017. Ice dices for monitoring stream surface velocity. J. Hydroenviron. Res. 14, 143–149. https://doi.org/10.1016/j.jher.2016.09.001.

Tazioli, A., 2011. Experimental methods for river discharge measurements: comparison among tracers and current meter. Hydrol. Sci. J. 56 (7), 1314–1324. https://doi.org/10.1080/02626667.2011.607822.

Vandenbohede, A., Louwyck, A., Lebbe, L., 2009. Conservative solute versus heat transport in porous media during push-pull tests. Transport Porous Media 76 (2), 265–287. https://doi.org/10.1007/s11242-008-9246-4.

Zhang, G.H., Luo, R.T., Cao, Y., Shen, R.C., Zhang, X.C., 2010. Correction factor to dye-measured flow velocity under varying water and sediment discharges. J. Hydrol. 389 (1–2), 205–213. https://doi.org/10.1016/j.jhydrol.2010.05.050.

Zhuang, X., Wang, W., Ma, Y., Huang, X., Lei, T., 2018. Spatial distribution of sheet flow velocity along slope under simulated rainfall conditions. Geoderma 321, 1–7. https://doi.org/10.1016/j.geoderma.2018.01.036.